Dual-layered nanocomposite membrane incorporating graphene oxide and halloysite nanotube for high osmotic power density and fouling resistance

Sungil Lim[1], Myoung Jun Park[1], Sherub Phuntsho[1], Anne Mai-Prochnow[2], Anthony B. Murphy[2], Donghan Seo[2] and Hokyong Shon[1] *

[1] *Centre for Technology in Water and Wastewater (CTWW), School of Civil and Environmental Engineering, University of Technology Sydney (UTS), Australia*

[2] *Commonwealth Scientific and Industrial Research Organisation (CSIRO) Manufacturing, Australia*

[*] Corresponding author: Professor Hokyong Shon, Email: hokyong.shon-1@uts.edu.au; Tel.: +61 2 9514 2629; Fax: +61 2 9514 2633.

Abstract

This study introduces a thin-film composite (TFC) membrane with a dual-layered nanocomposite substrate synthesized using a dual-blade casting approach for application in osmotic power generation by the pressure-retarded osmosis (PRO) process. The approach incorporates halloysite nanotubes (HNTs) into the bottom polymer substrate layer and graphene oxide (GO) on the top layer substrate, on which a thin polyamide active layer is formed. The fabricated membrane substrate showed highly desirable membrane substrate properties such as a high porosity, opened-bottom surface, suitable top-skin surface morphology for subsequent active layer formation and high mechanical strength, which are essential for high-performance PRO processes. At a GO loading of 0.25 wt% and HNT loading of 4 wt%, the power density (PD) of the nanocomposite membrane was 16.7 W/m^2 and the specific reverse solute flux (SRSF) was 2.4 g/L operated at 21 bar applied pressure using 1 M NaCl as draw solution and deionized water as feed, which is significantly higher than the those for a single-layered or commercial PRO membrane. This membrane performance was observed to be stable in the pressure cycle test and under long-term operation. The membrane substrate with HNTs incorporated exhibited high fouling resistance to sodium alginate and colloidal silica foulants, with the PD decreasing by 17% after 3 h of operation, compared to a membrane substrate without HNTs and commercial PRO membranes, which decreased by 26% and 57%, respectively. A fluorescence microscope study of the membranes subjected to feed water containing *Escherichia coli* confirmed the good antibacterial properties of the dual-layered TFC membrane. The study provides an attractive alternative approach for developing PRO membranes with high PD and fouling resistance.

Keywords: Dual-blade casting; nanocomposite membrane; graphene oxide; halloysite nanotube; pressure-retarded osmosis.

1. Introduction

The increasing demand for energy in the world has led researchers to search for renewable energy from various natural sources. Currently, the sources of renewable energy include biomass and waste (75%), hydro (17%) and wind and solar power (6%) [1]. The free energy released by mixing water with different salinities, such as when river water mixes with ocean water, has recently gained renewed interest as a reliable source of renewable natural energy [1, 2]. Membrane technologies such as pressure-retarded osmosis (PRO) and reverse electrodialysis (RED) are being investigated for harvesting osmotic-gradient energy from the salinity differences. PRO is seen as more attractive than RED because it allows high efficiency of energy harvesting, and is more suitable for operation under high salinity gradient [3]. In contrast to other renewable energy sources, the PRO process is not strongly affected by weather or climate phenomena, and is able to produce energy for 24 h per day under appropriate operating conditions [4]. The total estimated osmotic power globally at the points where rivers discharge into oceans could reach 2000 TWh/year. [3]. One of the potential applications of the PRO process is energy generation using reverse osmosis (RO) brine in a hybrid system combined with RO seawater desalination. This system is able to produce renewable energy using the RO brine as a draw solution and treated wastewater as a feed solution. This not only lessens the net RO energy consumption by producing energy from the PRO process, but also mitigates detrimental issues related to RO brine disposal by diluting the brine [5].

Loeb and his colleagues first conceptualized the PRO process in the 1970s. Although interest in the process has recently been revitalized for renewable energy production applications, the technology still suffers from a lack of suitable semi-permeable osmotic membranes that have the required output for energy production [5-7]. An analysis by the Norwegian company Statkraft,

which built a prototype plant in 2009, found that the power density (PD) of the membrane should be at least 5 W/m^2 for the PRO process to be commercially viable for producing net energy [3, 5, 7, 8]. An ideal PRO membrane must possess high water permeability, ion selectivity and mechanical strength, which together produce a high PD in PRO processes. The thin, active layer of the PRO membrane must be supported by a strong and yet highly porous membrane substrate in order to have a high PD. However, a tradeoff exists between the substrate porosity and the mechanical strength of the membrane [3, 9, 10]. Further, the development of PRO membranes must also consider its resistance to fouling propensity [9, 11-14]. When the membrane operates in the orientation with its active layer facing the draw solution (AL-DS), the organic matter, scaling precursors and other foulants contained in the feed solution can easily foul the membrane surface facing the porous substrate, resulting in a significant PD decline [11, 14-17]. Inorganic scaling such as that due to calcium salts can be controlled by adjusting pH and using anti-scalants. However, organic and colloidal fouling is a major concern in the PRO process; it can significantly reduce membrane permeability and hence PD due to the accumulation of foulants inside the membrane substrate (internal fouling) [11, 14].

Many strategies have been proposed to fabricate a better membrane substrate to improve the performance of PRO membranes. As noted above, water permeability and mechanical strength are two crucial properties that have been considered. A number of polymer-based materials (e.g., polyamide-imide, polyetherimide, modified polyethersulfone) and nanomaterials such as carbon nanotubes (CNTs) have been used in membranes in order to reduce membrane structural deformation while retaining high water flux under high-pressure PRO operation [4, 18-20]. In a different approach, She et al. [21] investigated the effect of a backing support in fabric-reinforced PRO membranes using non-woven, woven and tricot fabric, and inferred that related mechanisms

affected the membrane deformation under high hydraulic pressure conditions. Cheng et al. [10, 22] and Le et al. [23] developed outer-selective hollow-fiber PRO membranes, which are superior in terms of collapsing membranes and bursting fibers in inner-selective membrane modules under PRO operation.

Modification of the membrane surface is a new approach to mitigate membrane fouling. Many modification methods have been reported, such as coating with a hydrophilic [24, 25] or hyper-branched polymer [26, 27], depositing double-skinned selective layers [28], and layer-by-layer approaches on the membrane substrate [29]. The modification of the membrane surface aims to enhance its interaction using water-induced electrostatic repulsion [11, 27, 28, 30]. Although the surface-modified membranes exhibit lower fouling potential in their initial stage, the fouling resistance can deteriorate with operation time due to the physico-chemical damage caused by membrane fouling and chemical cleaning [30].

In previous studies, the co-casting method has been successfully applied to develop dual-layered membrane substrates with a high-porosity, opened-bottom surface and desirable surface morphology for subsequent polyamide (PA) formation on the surface [31-34]. As a result, these membranes exhibited high water flux and salt rejection due to the alleviation of internal concentration and thus polarization in osmotically driven processes. Liu et al. [32] introduced dual-layered mixed-matrix membranes with the addition of colloidal silica to further enhance the membrane's performance. In particular, a high loading of colloidal silica ranging from 0 to 4 wt% was thoroughly impregnated into the bottom layer, forming a void-free top surface, which is an ideal morphology for PA layer formation. However, it is important to note that the approach used for the dual-layered membrane substrate should take into account the trade-off that exists between the membrane substrate porosity and its mechanical strength for PRO application. In addition, the

113 dual-layered membrane substrate has a propensity for membrane fouling on the porous bottom
114 layer when it is exposed to the feed stream in the PRO operation.

115 Hydrophilic nanomaterials have been applied to improve the membrane's physico-
116 chemical properties. One example is the incorporation of graphene oxide (GO) nanosheets into
117 single- and dual-layered polysulfone (PSf) substrates to improve the substrates' porosity and
118 hydrophilicity [34-37]. The use of GO nanosheets results in a smoother substrate surface
119 morphology that assists in the desirable formation of a PA active layer [34, 37]. In another example,
120 naturally formed halloysite nanotubes (HNTs) were used for the modification of polymer materials
121 [38, 39]. HNTs are novel 1D tubular nanostructures with large aspect ratio and high mechanical
122 strength [38, 39]. HNTs are easily produced from natural sources that are abundant worldwide and
123 are much cheaper than other nanomaterials such as CNTs, GO and titanium oxide (TiO_2). Further,
124 it has been reported that a polymer–HNT nanocomposite possesses highly increased tensile and
125 flexural strength and elastic modulus [38]. The fragments of HNTs are well dispersed in various
126 polar, non-polar solvents and polymeric liquids because of the relatively weak tube-to-tube
127 interactions, in contrast to CNTs [40, 41]. Furthermore, HNTs have similar functionality to
128 functionalized CNTs because of their hydrophilicity and nanoscale geometry. Kang et al. [42]
129 reported that functionalized multi-wall CNTs (fCNTs) showed a bacterial cytotoxicity against
130 *Escherichia coli* because of their physico-chemical properties. Therefore, the incorporation of GO
131 and HNTs into polymeric membranes is expected to enhance not only the flux but also its fouling
132 resistance for the PRO process.

133 The current work therefore aimed to develop a novel dual-layered GO/HNT nanocomposite
134 osmotic membrane with high PD and high fouling resistance for osmotic power generation by the
135 PRO process. These PRO membranes were prepared using an optimum GO loading in the top layer

and HNT loading in the bottom layer of the membrane substrate. The performance of these dual GO/HNT layered membranes was compared with the single- or dual-layered PRO membranes prepared with or without GO and HNTs and with a commercial TFC PRO membrane. To the best of our knowledge, this is the first work to report the development of a novel PRO membrane using GO/HNT layers with the aim of improving its performance and fouling resistance. The findings from this study are expected to significantly contribute towards the application of the PRO processes for osmotic power generation from the natural salinity gradient.

2. Experimental

2.1 Materials and chemicals

Polysulfone (PSf, Udel 3500, Solvay) was used as a polymer for the preparation of membrane substrates with 1-methyl-2-pyrrolidone (NMP, Merck) as solvent mixed with polyethylene glycol with molecular weight 400 (PEG 400, Sigma-Aldrich) as an additive. 1,2-phenylenediamine (MPD, Sigma-Aldrich) and trimesoyl chloride (TMC, Sigma-Aldrich) were used as monomers for forming a polyamide layer on the membrane substrate by interfacial polymerization. N-hexane (Merck) with the highest purity of 98% was used as the solvent for TMC. Sodium chloride was used as the draw solute in the PRO performance tests and salt permeability tests with deionized water with resistivity of 18 MΩ/cm (Milli-Q, Millipore) as the feed solution. GO nanosheets and HNTs (Halloysite nanoclay, Sigma-Aldrich) were incorporated into polymer solutions for the substrate fabrication. It is confirmed by the manufacturer (Sigma-Aldrich) that the inner diameter and total length of the HNTs are 30 – 70 nm and 1 – 3 μm, respectively. GO nanosheets were synthesized via the Hummer's method; the preparation details can be found in

158 our previous studies [37]. Membrane fouling tests were conducted using a synthetic feed solution
159 containing model foulant such as 200 mg/L of alginate (Sodium Alginate, Sigma-Aldrich) and 200
160 mg/L of colloidal silica (ST-ZL, 100 nm, Nissan Chemical) mixed into the deionized water. The
161 commercial TFC PRO membranes were obtained from Toray Chemical, Republic of Korea. The
162 polyethylene terephthalate (PET) woven fabric mesh (07-105/52, Sefar) was applied as a backing
163 support to reinforce the membrane substrates.

164

165 ***2.2 Preparation of nanocomposite membrane substrates***

166 All membrane substrates were fabricated by the phase inversion method. Polymer solutions
167 were prepared by simultaneously mixing PSf, NMP, PEG 400 and GO nanosheets or HNT
168 nanotubes in a dried glass bottle at 60°C for 24 h using a magnetic stirrer. GO nanosheets were
169 thoroughly dispersed in a NMP solution by sonication for more than 12 h prior to the mixing of
170 polymer solution. Subsequently, the well-mixed polymer solutions were filtered using 85 μm PET
171 mesh (07-85/46, Sefar) and then de-gassed in a vacuum chamber at 30 °C for more than 3 h before
172 being cast on the glass plate. A dual-blade casting approach was used for preparation of dual-
173 layered membrane substrates with different polymer concentration and thickness [31, 33]. As
174 presented in Fig. 1, two substrate layers were simultaneously cast on the backing fabric using an
175 automatic casting machine (Elcometer 4340, Elcometer Asia Pte Ltd.) with two different blades
176 (blade 1 with 0 μm casting thickness for the bottom layer and blade 2 with 180 μm casting
177 thickness for the top layer) and different compositions of polymer (top layer with PSf at 18 wt%
178 and PEG at 10 wt%, and bottom layer with PSf at 9 wt%). The actual thicknesses were optimized
179 at 63 μm for the bottom layer, which is equivalent to the thickness of the PET backing support,

and 180 μm for the top layer formation. The detailed casting conditions for the substrates are shown in Table 1.

For the preparation of the dual-layered PSf/GO substrate, the optimum GO nanosheet dosing ratio of 0.25 wt% was used as it had been found favorable for subsequent polyamide layer formation in our previous work [37]. PSf solutions for the bottom layer were mixed with different dosages of HNTs ranging from 0 to 6 wt%, aiming to enhance mechanical strength, improve water permeability during PRO operation and mitigate membrane fouling on the bottom surface.

All membrane substrates were cast on the woven fabric mesh supported on the glass plate. The woven fabric backing support was used for enhancing mechanical strength of the membrane substrate. After the polymer film was cast on the glass plate, it was immediately immersed into a water coagulation bath at room temperature (23°C) for 30 min. Nascent membrane substrates were then stored in deionized (DI) water for about 24 h to allow complete removal of residual solvents. Table 1 shows the different compositions of polymer (PSf) and nanomaterials (GO and HNTs) used for the preparation of dual-layered PRO membrane substrates. The single-layered and dual-layered PSf membrane substrates prepared as a control without any nanomaterials are denoted as *S/free* and *D/free*, respectively. In addition, dual-layered PSf nanocomposite membranes were prepared with GO at 0.25 wt% in the top layer and HNTs in bottom layer at the concentrations of 0, 2, 4 and 6 wt%. The membrane substrates were given the name *GO/HNT0* to *GO/HNT6* depending on the concentration.

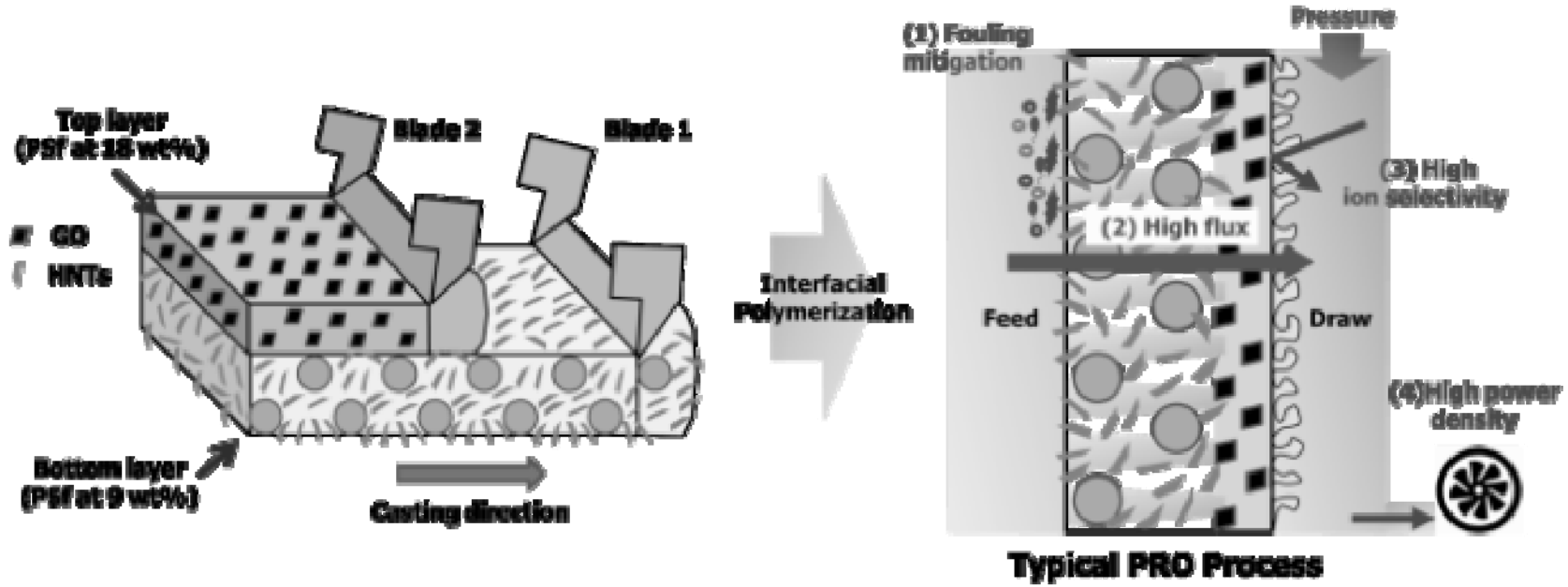

199

200 **Figure 1** Conceptual illustration of the dual-layered TFC PRO membranes with GO and HNTs incorporated in the top and bottom
201 substrate layer, respectively. The optimum PRO membrane in this study is expected to possess high PD, high ion selectivity and
202 significant fouling resistance for osmotic power generation.

203

Table 1 Compositions of polymer solutions for the fabrication of the PRO membrane substrates.

Membrane substrates	Top layer (wt%)				Bottom layer (wt%)		
	PSf	PEG 400	GO loading	NMP	PSf	HNTs loading	NMP
S/free	18	10	-	72	-	-	-
D/free	18	10	-	72	9	0	91
GO/HNT0	18	10	0.25	72	9	0	91
GO/HNT2	18	10	0.25	72	9	2	91
GO/HNT4	18	10	0.25	72	9	4	91
GO/HNT6	18	10	0.25	72	9	6	91

* The weight percentages of nanomaterials (GO and HNTs) were calculated relative to the mass of the PSf.

2.3 Formation of thin-film composite membranes

A selective polyamide (PA) layer was formed on the surface of the top membrane substrate (skin layer) based on the reaction of water-based MPD and organic-based TMC via the interfacial polymerization process. The detailed method for the process is presented in the supporting information (SI). The prepared TFC membrane samples in this study were denoted by *T-name of the membrane substrate*, and the commercial PRO membrane was named *CPRO*.

2.4 Membrane characterizations

The morphological structures of both the surface and cross-section of the membranes were observed with a field emission scanning microscope (FE-SEM, Zeiss Supra 55VP, Carl Zeiss AG) operated at 5 to 10 kV. Most of the samples were fully dried with a compressed N_2 gas. To perform cross-section analysis, all membrane samples were rapidly frozen in liquid nitrogen and fractured. Before imaging using the FE-SEM, all samples were coated with platinum and gold using a sputter coater (EM ACE600, Leica).

The porosity of the membrane substrates was indirectly determined via the difference between the weights of the membranes in wet and dry condition. The methodology has been presented previously [43]. The chemical properties of the HNTs in membrane substrates were investigated using Fourier transform infrared spectroscopy (FTIR, Affinity-1, Shimadzu). The signal was detected in the range of 500–4000 cm^{-1} with a signal resolution of 1 cm^{-1} and a minimum of 16 scans. The contact angles of the membranes were measured by the sessile drop method using the optical subsystem (Theta Lite 100, Biolin Scientific) equipped with image-analysis software. The contact angle for each sample was determined by averaging data from five measurements in random positions. The topography and roughness of the substrate membranes were characterized using atomic force microscopy (Dimension 3100, Veeco). The surface of the substrate membranes was scanned at 5 μm in tapping mode in ambient atmosphere. The measurements were repeated at least three times.

The mechanical strength of the membrane substrates was evaluated by a Materials Testing Machine (Lloyd-LS, Lloyd, UK) with a 1 kN load cell at a constant crosshead speed of 5 mm/min. The samples were tailored at 1 cm in width and 3 cm in length. For the mechanical tests, both fabric-based membranes and fabric-free membranes were tested to accurately evaluate the mechanical enhancement of membrane substrates with HNTs embedded. The thickness of both membranes was in the range of 90 to 110 μm, and tensile strength, stress at break, strain at break and the strain–stress curve were determined in the test.

To evaluate the intrinsic transport properties of TFC PRO membranes, the pure water permeability (A, L m^{-2} h^{-1} bar^{-1}) and solute permeability coefficient (B, L m^{-2} h^{-1}) were measured using a cross-flow RO test unit with an effective membrane area of 20.02 cm^2. The methods for evaluating the values of A and B are given in the SI.

2.5 Evaluation of TFC PRO membrane performance

2.5.1 Water flux, reverse solute flux and power density

The performance of the PRO membranes was tested using the laboratory-scale PRO test unit shown in Fig. S1. The orientation of the membrane in the test was AL-DS (active layer facing draw solution) under an applied hydraulic pressure in the draw stream that was varied from 0 to 27 bar. The detailed methods for determining the key performance parameters (water flux, reverse solute flux, SRSF and PD) are presented in the SI.

2.5.2 Membrane stability in PRO operation

The reversibility and long-term operating tests of the PRO membranes were conducted to provide a more reliable evaluation of their performance. The reversibility tests were conducted in two rounds of PD tests with an increase of the applied pressure up to 27 bar. A comparison of PD in the first and the second round was made as a function of the applied pressure. In addition, the PRO membranes were operated for 5 h at the applied pressure for which the PD reached the highest value in the tests.

2.6 Fouling and anti-biological tests of TFC PRO membranes

A model feed solution containing colloidal silica, serving as nano-sized particulates, and sodium alginate, representing an organic foulant, was used in the fouling tests. These tests were

used to investigate the influence on the performance of the PRO membrane of the deposition on membrane substrates of foulants in the feed solution. Baseline tests were carried out prior to the fouling tests to acquire benchmarking data for comparison. The baseline tests were run for 30 min with 1 M NaCl draw solution and DI water feed solution. Colloidal silica at 200 mg/L and sodium alginate at 200 mg/L were spiked into the DI water, and the spiked feed solution was circulated in the feed stream for the fouling test.

To investigate the antibacterial properties of the membrane samples, the particle-free (*S/free*) and nanocomposite (*GO/HNT4*) membranes were selected to be tested for *Escherichia coli* K12 (MG 1655; Food Research Ryde Bacteriology Culture Collection) attachment. *E. coli* was grown overnight in nutrient broth (1g/L `Lab-Lemco' powder, 2g/L yeast extract, 5g/L peptone, 5g/L sodium chloride, pH 7.4; Oxoid) at 37°C to an optical density of 1. A 5 μL aliquot of overnight culture was inoculated into 1 mL of fresh nutrient broth in a well of a 24-well tissue culture plate. Each well also contained a 1 cm^2 piece of submerged membrane sample. The 24-well plate was incubated for 16 hours at 37°C with slight shaking (80 rpm). To investigate bacterial attachment, the membrane samples were stained with the BacLight Live/Dead stain containing the 2 stock solutions green Syto 9 and red propidium iodide (Molecular Probes, Eugene, Oregon, USA) according to the manufacturer's instructions. Cells on the membranes were visualized in the tissue culture plates using an Olympus IX83 inverted microscope equipped with CellSense imaging software.

3. Results and discussion

3.1 Characteristics and performances of membrane substrates

Fig. S2 presents the ATR-FTIR spectra of dual-layered membrane substrates incorporated with GO and HNTs for PRO application. Compared to the HNT-free membrane (*D/free*), the spectra of HNT-incorporated membranes show two new peaks at 915 and 1033 cm^{-1}. The peaks at 915 and 1033 cm^{-1} represent the single aluminum hydroxyl bonding compounds (Al-OH) and the asymmetric stretch vibration of siloxane (Si=O=Si), respectively. The peak intensities increase with HNT concentrations, and they are largest in the spectrum of membrane *GO/HNT6*. The presence of the two additional peaks verifies that the HNTs were well incorporated into the bottom layer of the dual-layered PRO membrane substrates.

The field emission-scanning electrode microscopy (FE-SEM) images of the top surface, bottom surface and cross-section of the PRO membrane substrates are shown in Fig. 2. While it is possible for the HNTs to diffuse from the bottom to the top layer of the GO/HNT membrane substrates in a phase inversion, it is evident from the SEM images that the top surfaces of most membrane substrates show an HNT-free, dense skin layer, which is desirable for the formation of a PA selective layer. However, some HNT shapes were observed on the top surface of *GO/HNT6* membrane, indicating that some of HNTs fully penetrated the top layer of the membrane substrate, likely due to the high dosing ratio. The presence of HNTs on the top surface could cause defects for subsequent PA layer formation [44]. The bottom surfaces of dual-layered membrane substrates exhibit a much more porous structure than that of the single-layered membrane substrate, with small pores in the clusters. For the dual-layered PRO membrane substrates, however, the pore size and pore density of the bottom surface are slightly decreased with increasing HNT loading. This

304 is evident from the bottom morphology of *GO/HNT6*, which is less porous than that of the
305 membrane without HNTs (*GO/HNT0*). At relatively high concentrations of HNTs, this is likely to
306 hinder the solvent and water exchange during the phase inversion process due to the high viscosity
307 of the polymer solution and hence lead to the formation of a less-porous bottom surface [45]. In
308 particular, some HNT fragments could partially block the pores and lay across the pores, as
309 presented in Fig. S3. Interestingly, this shows that the morphological pattern of the bottom surface
310 of membrane substrates could be controlled by varying the HNT loading. This approach could be
311 beneficial in mitigating foulant penetration from the feed stream into pores of membrane substrate
312 by altering the surface morphology of the membrane substrate.

313 The cross-sectional images of PRO membranes in pristine condition and in pressurized
314 condition after PRO operation are shown in Fig. 2. A close observation of the SEM images
315 indicates that the dual-layered membrane substrates mainly exhibit finger-like macropores, while
316 single-layered membranes exhibit both finger-like voids and sponge-like structures. Although the
317 porous structure of the membrane substrate is able to mitigate internal concentration polarization
318 in osmotically driven processes, it is necessary to evaluate the mechanical properties of the
319 membrane substrate when subjected to high hydraulic pressure during PRO operation. Comparison
320 of the cross-sectional SEM images of membranes taken before and after the PRO operation shows
321 that the *S/free* and *GO/HNT4* membranes were less compressed compared to other dual-layered
322 membranes, for which the morphology of the membrane substrates appeared slightly deformed.

323 Table 2 presents a summary of the physical properties of the PRO membrane substrates
324 prepared in this study. The morphological structures were well correlated with the porosity. The
325 porosity of all dual-layered membrane substrates was around 66%, which is higher than that of
326 single-layered substrate, which was around 60%. Our results and previous studies show that the

double-blade casting method is a promising candidate to prepare porous membrane substrates [31-33]. The mechanical properties of all membrane substrates were similar in terms of tensile strength, stress at break and strain at break, despite differences in the structural morphologies and the porosity. This indicates that the mechanical strength of the PRO membrane substrate is likely to be attributed to the woven fabric mesh backing incorporated into membrane substrates instead of the substrate polymer.

To support this argument, fabric-free membrane substrates under similar compositions were prepared, and their mechanical strength was compared. Fig. 3 presents the strain–stress curve (a) and tensile strength (b) of fabric-free flat-sheet PRO membrane substrates. The mechanical strength of the membrane substrates gradually increased with the increase in HNTs concentration up to 4 wt%. The tensile strength of the *GO/HNT4* membrane at 2.81 MPa was higher than that of the *GO/HNT0* membrane at 2.21 MPa, indicating HNTs play an important role in enhancing the mechanical strength of the polymer-based membrane structure. However, at an HNT concentration over 4 wt%, the mechanical strength of the membrane substrate dropped significantly, likely due to the weakening the substrate's physical structure by the aggregation of HNTs in the polymer structure at excess dosage [38]. Fig. S3 also shows the presence of HNTs inside the PRO membrane substrate at higher SEM magnification. The HNTs appear well distributed in both the *GO/HNT2* and *GO/HNT4* membrane substrates; however, some clusters of aggregated HNTs were observed inside the *GO/HNT6* substrate due to over-dosing of HNTs. Based on these findings, it is evident that the HNT loading at 4 wt% in the polymer solution is the optimum composition for improving the mechanical strength of a PRO membrane substrate. Nevertheless, the fact that there are significant differences in the mechanical properties of the fabric-free membranes, but not in

the membranes with the fabric mesh backing, supports the contention that the mesh backing is the main source of the mechanical strength of the PRO membranes.

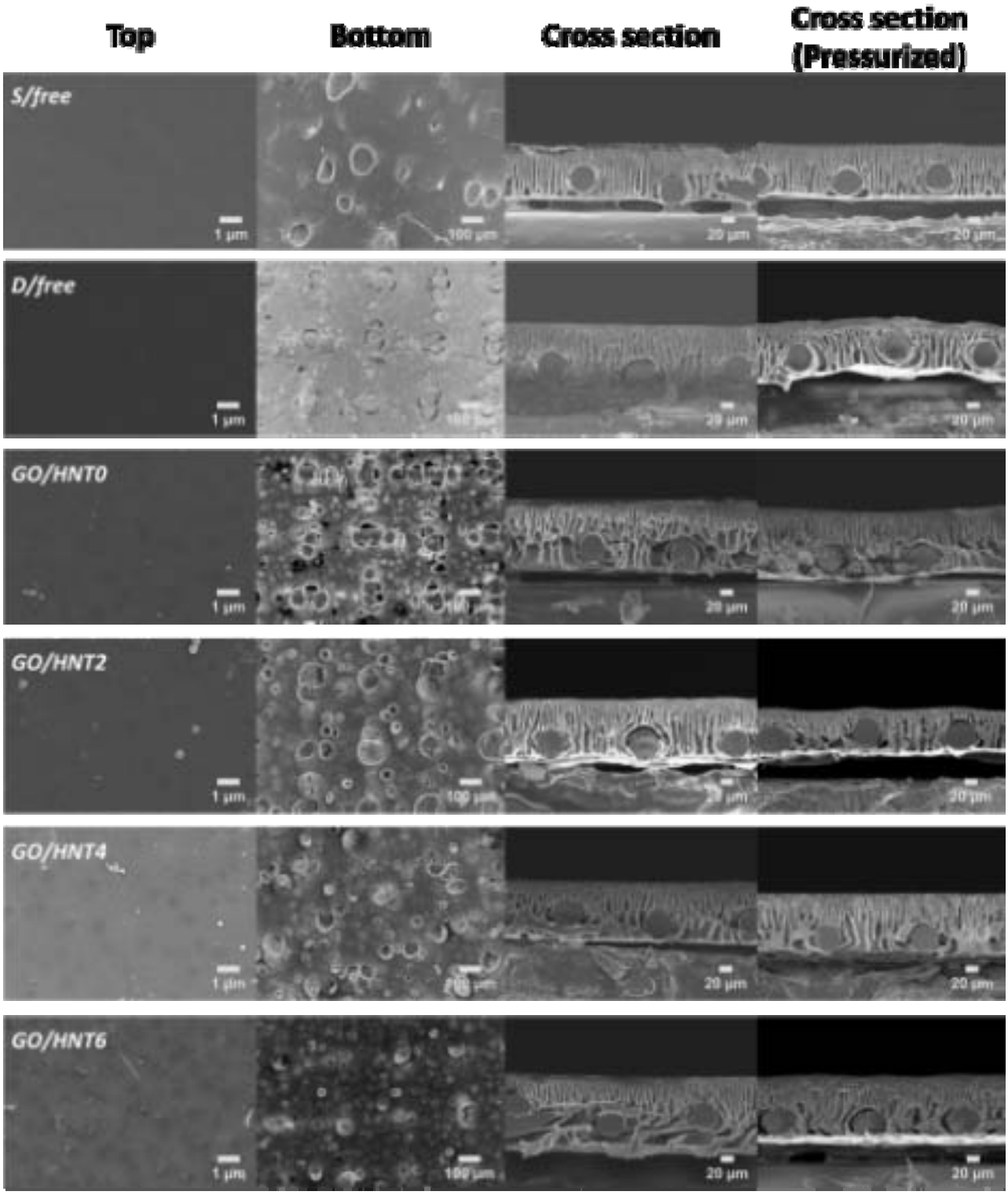

Figure 2 SEM images of flat-sheet PRO membrane substrates: Top, bottom and cross-section morphologies, and cross-section morphologies for pressurized membrane substrates under the applied pressure of up to 27 bar.

Table 2 Physical properties of PRO membrane substrates.

Substrates	Porosity of substrate (%)	Thickness (μm)	Tensile strength (MPa)	Stress at break (MPa)	Strain at break (%)
S/free	60.6 ± 0.6	89.8	36.2 ± 2.1	34.6 ± 3.8	22.9 ± 4.0
D/free	66.3 ± 0.7	103.1	35.8 ± 6.7	33.9 ± 7.6	23.0 ± 4.8
GO/HNT0	66.5 ± 1.2	101.8	36.0 ± 2.9	32.9 ± 3.0	20.6 ± 2.5
GO/HNT2	66.2 ± 0.4	104.2	35.1 ± 4.8	31.3 ± 2.9	19.5 ± 0.2
GO/HNT4	66.8 ± 0.1	103.5	36.1 ± 6.6	33.1 ± 7.7	21.1 ± 3.5
GO/HNT6	66.8 ± 0.4	107.5	35.1 ± 5.3	32.2 ± 5.9	21.0 ± 3.5

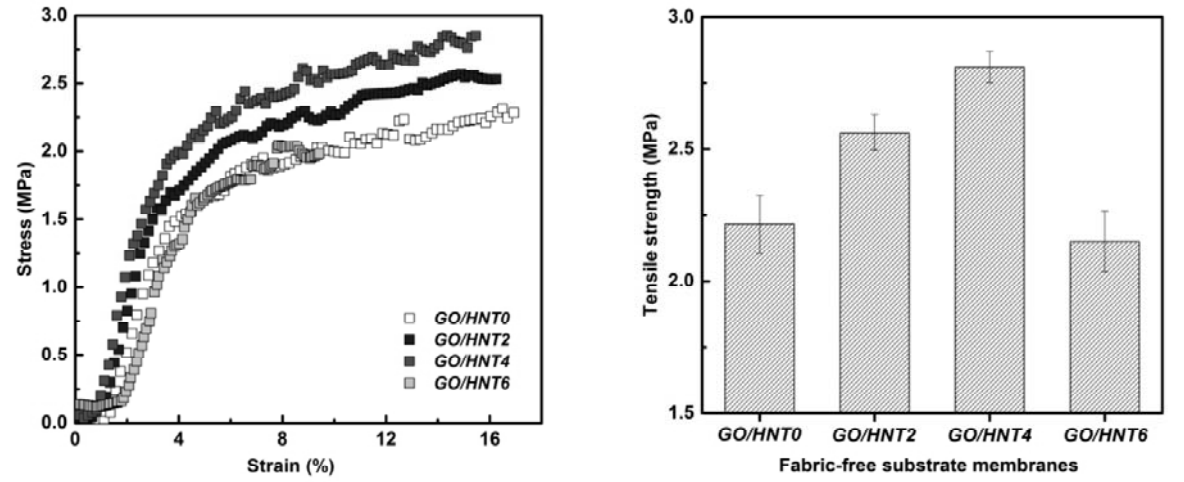

(a) (b)

Figure 3 Strain–stress curve (a) and tensile strength (b) of fabric-free flat-sheet PRO membranes. The concentration of HNTs was varied from 0 to 6 wt%. The actual thickness of the membranes ranged from 95 to 110 μm.

In the design of the dual-layered PRO membrane, the HNTs mixed with PSf in the bottom-layer substrate are expected to have anti-biological activity as well as improved mechanical strength, especially those HNT fragments that are exposed on the bottom surface of the membrane substrate. The presence of exposed HNTs on the membrane surface is expected to provide a higher bottom surface roughness. HNTs on the membrane surface can act as a nano-blade. Thus the spinescent morphology of the bottom surface of the dual-layered membrane substrate was designed to physically damage (pierce) microorganisms that come into contact with the bottom surface. 3D AFM images and measurements of the average roughness of the bottom layers of the PRO membrane substrate presented in Fig. S4(a) show a slightly higher than average roughness of membrane substrates at increased HNT concentrations. The bottom surface of the *GO/HNT6* membrane exhibited the highest average roughness, 30.82 nm, of all the substrates. The contact angle data of the bottom layer of the membrane substrates shown in Fig. S4(b) support the AFM measurements by showing higher contact angle for the membrane substrates with higher HNT concentrations. The rough morphology of the membranes with embedded HNTs likely results from the protrusion of HNTs to the surface, possibly forming a hill and valley surface morphology, which increases the contact angle of a water droplet due to the existence of air pockets [46]. These results indicate that HNTs could play a significant role in controlling the roughness of the bottom layer of the membrane substrates.

3.2 Characteristics and performance of TFC PRO membranes

3.2.1 Intrinsic transport properties of TFC PRO membranes

382 The intrinsic transport properties of the PRO membranes such as water permeability (*A*)
383 and solute permeability (*B*) were determined in the RO mode of operation at 5 bar applied pressure.
384 In addition, the intrinsic selectivity (*B/A*) and NaCl rejection of the PRO membranes is shown in
385 Table 3. The intrinsic selectivity of the PRO membranes was defined as the ratio of the solute
386 permeability and water permeability. The selectivity of ideal TFC membrane should be minimized,
387 which means that a high *A* value and a low *B* value are desirable.

388 Table 3 shows that the *B/A* values of the *T-S/free*, *T-D/free* and *T-GO/HNT0* TFC
389 membranse were similar, indicating that their membrane surface morphologies were similar for
390 subsequent PA formation. However, with the addition of HNTs into the dual-layered substrate, the
391 *B/A* values of *T-GO/HNT2* and *T-GO/HNT4* declined significantly (up to 0.17 bar) compared to
392 *T-D/free.* This can be attributed to the high water permeability and the strong substrates that retain
393 the integrity of the PA layer very well under pressure. In addition, NaCl rejection was found to be
394 correlated to the *B/A* value. While the *A* value of *GO/HNT6* reached the highest value of 2.40
395 LMH/bar for HNT loading at 6 wt%, the *B* value rose significantly to 0.72 LMH, the highest value
396 among all nanocomposite membranes, which is undesirable for a membrane. The high loading of
397 HNTs at 6 wt% likely results in the decline of the degree of PA cross-linking under the IP process.
398 The presence of HNTs on the top surface of the membrane surface is shown in Fig. 2. Consequently,
399 undesirable voids or cracks in the PA layer occurred, which gave rise to poor solute selectivity.
400 Therefore, *T-GO/HNT4* possessed the lowest *B/A* value of 0.17 bar, which is an optimum
401 parameter for a membrane performance. It is notable that, due to the presence of HNTs, the best
402 intrinsic transport properties for all TFC membranes tested, including the commercial membrane,
403 were found in *T-GO/HNT4*. The *B/A* value of *T-GO/HNT4* is half that of the commercial PRO

(*CPRO*) membrane (0.36 bar), which indicates that the fabricated TFC PRO membranes exhibited better performance than state-of-the-art *CPRO* membranes.

Table 3 Intrinsic transport properties of homemade and commercial TFC PRO membranes: pure water permeability (*A*), solute permeability (*B*), intrinsic selectivity (*B/A*) and NaCl rejection. The properties were determined by a cross-flow operation at 5 bar.

TFC PRO membranes	*A* ($Lm^{-2}h^{-1}bar^{-1}$)	*B* ($Lm^{-2}h^{-1}$)	*B/A* (bar)	NaCl rejection (%)
T-S/free	1.97±0.08	0.62±0.02	0.32±0.02	93.05±0.36
T-D/free	2.09±0.09	0.58±0.01	0.30±0.02	92.37±0.13
T-GO/HNT0	2.02±0.01	0.50±0.09	0.25±0.05	94.54±0.97
T-GO/HNT2	2.12±0.01	0.51±0.01	0.24±0.01	94.69±0.07
T-GO/HNT4	2.31±0.02	0.40±0.03	0.17±0.02	96.02±0.40
T-GO/HNT6	2.4±0.02	0.72±0.01	0.30±0.01	93.09±0.12
CPRO	1.85±0.05	0.66±0.08	0.36±0.05	92.25±0.98

3.2.2 Performance of TFC PRO membranes

3.2.2.1 Effect of GO in top layer of the membrane substrate on PRO performance

The PRO performance of the membrane samples was evaluated in terms of water flux, PD and SRSF at different applied pressures; the results are presented in Fig. 4. The GO-free single-layered membranes (*T-S/free*) exhibited a lower maximum PD, 7.2 W/m^2 at 18 bar, than the dual-layered PRO membranes. This observation is consistent with the porosity and pure water permeability of the *S/free* membrane substrate compared to those of other dual-layered samples

418 (Table 2). However, these single-layered membranes possess a high mechanical strength, which
419 helps to retain membrane support layer structure at high operating pressure of over 20 bar.

420 When the membrane substrate is prepared by the co-casting method to form a dual-layered
421 PSF substrate, the mechanical strength of the dual-layered control membrane decreases slightly
422 while its water permeability and PD increase due to its porous and opened-bottom structure, which
423 is not present in single-layered control membranes. The PD of *T-D/free* was 10.6 W/m^2, which is
424 higher than that of *T-S/free*. The PD of the dual-layered control membrane dropped sharply above
425 15 bar applied pressure, likely due to the compression and collapse of its porous support structure
426 (Fig. 4a). This is consistent with the significant increase in the SRSF of the dual-layered control
427 membrane from 2.89 g/L at 15 bar to 11.3 g/L at 27 bar shown in Fig. 4(b), which can be attributed
428 to the likely physical damage of the PA active layer due to uneven collapse of the porous support
429 structure under hydraulic pressure.

430 With the addition of GO into the top layer of the dual-layered membrane substrates, the
431 mechanical strength and PD of the TFC PRO membranes increased significantly, as evident from
432 the results for the *T-D/free* and *T-GO/HNT0* membranes presented above. The maximum PD for
433 the *T-D/free* was 10.6 W/m^2 at 15 bar, while for the *T-GO/HNT0* membranes it was 12.1 W/m^2 at
434 21 bar. In addition, the SRSF of *T-GO/HNT0* at the maximum PD was lower than that for the dual-
435 layered control membrane. These findings are consistent with previous studies, which showed that
436 the addition of GO into a polymer structure may provide additional advantages, including
437 improvement of the mechanical strength of the membrane substrates [47, 48]. The other notable
438 observation from Fig. 4 is the increase in the SRSF of all the TFC membranes at higher pressure
439 PRO operation. This occurs because the water flux is retarded by applied pressure, without

significantly affecting the solute concentrations across the membrane that determine the reverse solute flux (J_s).

The hysteresis of PD in the PRO membranes was investigated using a pressure cycle test in order to determine the stability and reversibility of the PRO membranes. A similarity of the PD in the first and second cycles indicates good stability and robustness of the PRO membranes. The applied pressure was increased from 1 to 21 bar in each cycle. The PD for *T-S/free* in each cycle was similar, as shown in Fig. 4(c), which indicates that the recovery of the PD was good, with its mechanical strength being able to withstand high applied pressures under PRO operation. However, the maximum PD was the lowest of the synthesized membranes. Unlike the *T-S/free* case, the PD of *T-D/free* in the first cycle increased with applied pressure to 15 bar, and then rapidly dropped. In the second cycle, the maximum PD fell significantly from 12.0 to 8.2 W/m^2 due to external damage to the membrane structure at applied pressures above 15 bar. The PD of *T-D/free* at pressures above 15 bar was similar in the first and second cycle due to the collapse of the membrane structure at these pressures. The PD of *T-GO/HNT0* in the second cycle at 21 bar (12.0 W/m^2) was marginally lower than in the first cycle (13.4 W/m^2). Although the addition of GO improved its hysteresis, the deformation of the membrane structure was irreversible under the test conditions used.

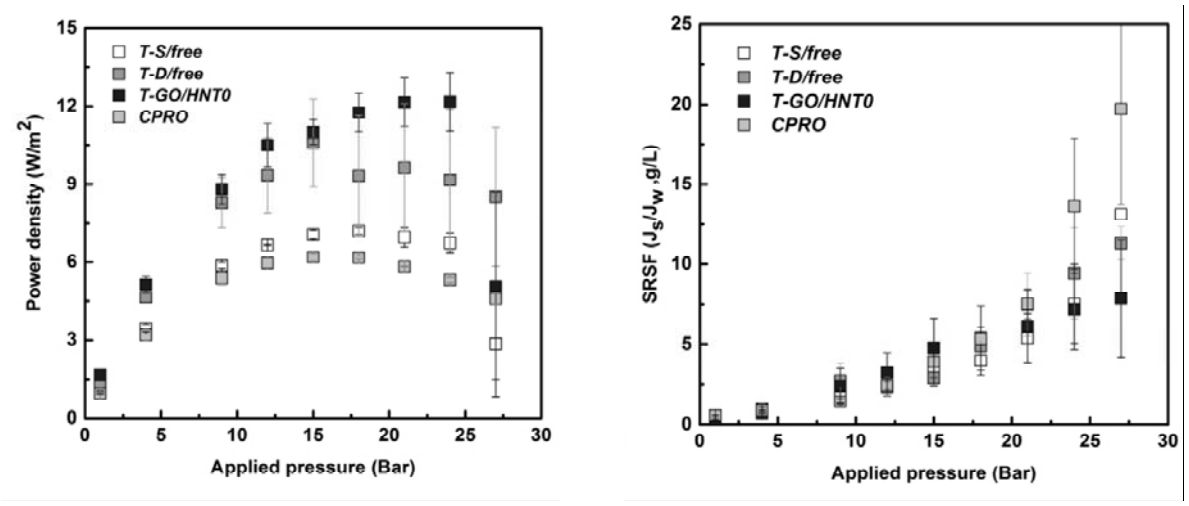

(a) (b)

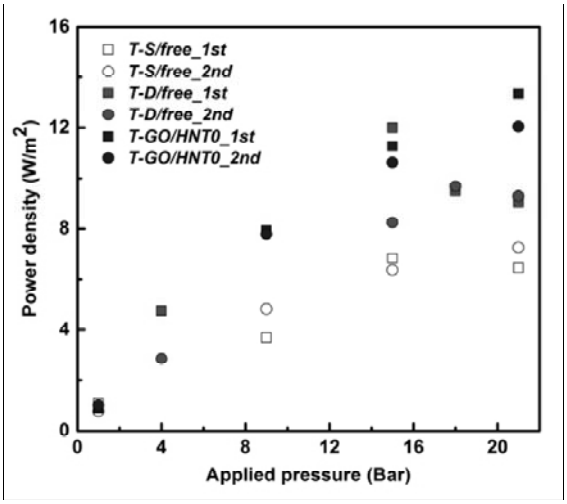

(c)

458 **Figure 4** (a) Power density (PD), (b) specific reverse solute flux (SRSF) and (c) pressure cycle
459 test of the PRO membranes at different applied pressures. The PD was determined from the water
460 flux and effective applied pressure. The feed and draw solutions were DI water and 1 M NaCl
461 solution, respectively.

462

463

464 *3.2.2.3 Effect of HNTs in the bottom layer of the dual-layered membrane substrate*

465 HNTs show a better dispersion in common solutions and polymers than other natural
466 silicates (such as kaolinite) and CNTs. Because HNTs have relatively few hydroxyl groups,
467 siloxane on their outer surface that have weak tube-tube interactions, and they have tubular
468 morphologies with a favorable aspect ratio that minimizes the contact between tubes [38, 39]. In
469 addition, the HNT loading in the bottom layer can be varied progressively, as the top layer is
470 capable of covering the bottom layer, with HNTs maintaining the suitability of the surface
471 morphology for subsequent PA formation [32]. However, the maximum concentration of HNTs in
472 the polymer mixture was limited due to the HNT aggregation. It is therefore necessary to find an
473 optimum HNT loading in order to fabricate the best PRO membranes.

474 Accordingly, the dosing ratio of HNTs was varied from 0 to 6 wt% in the bottom layer while the
475 GO concentration was fixed at 0.25 wt% in the top layer. Fig. 5 presents the PD and SRSF of the
476 *T-GO/HNT0* to *T-GO/HNT6* as a function of applied hydraulic pressure (0 to 27 bar). As shown in
477 the figure, the PD of *T-GO/HNT2* and *T-GO/HNT4* was over 16.7 W/m^2 at 21 bar, far better than
478 that of the other PRO membranes. Although the PD of the *T-GO/HNT4* (16.7 W/m^2) was slightly
479 lower than that of *T-GO/HNT2* (17.5 W/m^2), the SRSF of *T-GO/HNT4* (2.4 g/L) was significantly
480 lower than that of *T-GO/HNT2* (4.1 g/L) at the applied pressure of 21 bar. The enhanced PD and
481 solute selectivity of *T-GO/HNT4* mean that it exhibited excellent pressure tolerance, maintaining
482 its pore structure and support to its active layer on the membrane substrate under the highly
483 pressurized condition. However, with an HNT loading of 6 wt%, the maximum PD of *T-GO/HNT6*
484 dropped significantly to 10.7 W/m^2, accompanied by a strong rise in the SRSF. At a pressure of
485 18 bar, the SRSF of *T-GO/HNT6* was 6.5 g/L, which is around 3 times higher than that of *T-*
486 *GO/HNT4* (2.4 g/L). *T-GO/HNT2* and *T-GO/HNT4* also showed an excellent recovery of PD in

the pressure cycle test presented in Fig. 5(c); however, as expected, the PD of *T-GO/HNT0* and *T-GO/HNT6* noticeably decreased in the second cycle due to their poor mechanical properties. This suggests that HNT loading of 6 wt% or higher can lead to the formation of undesirable substrate morphology (voids, cracks or rough surface due to the aggregation of HNTs with themselves or with the polymer) which can undermine the membrane performance and its mechanical strength. As shown in the SEM images (Fig. 2), some of the HNT fragments are partially visible on the top surface of *T-GO/HNT6*, unlike the other membrane substrates, indicating that HNTs could penetrate to the surface at extremely high concentrations. These HNT fragments on the surface of the membrane substrate could be detrimental for subsequent PA formation. Our results confirm that the optimum HNT loading in the preparation of PRO membranes is around 4 wt%.

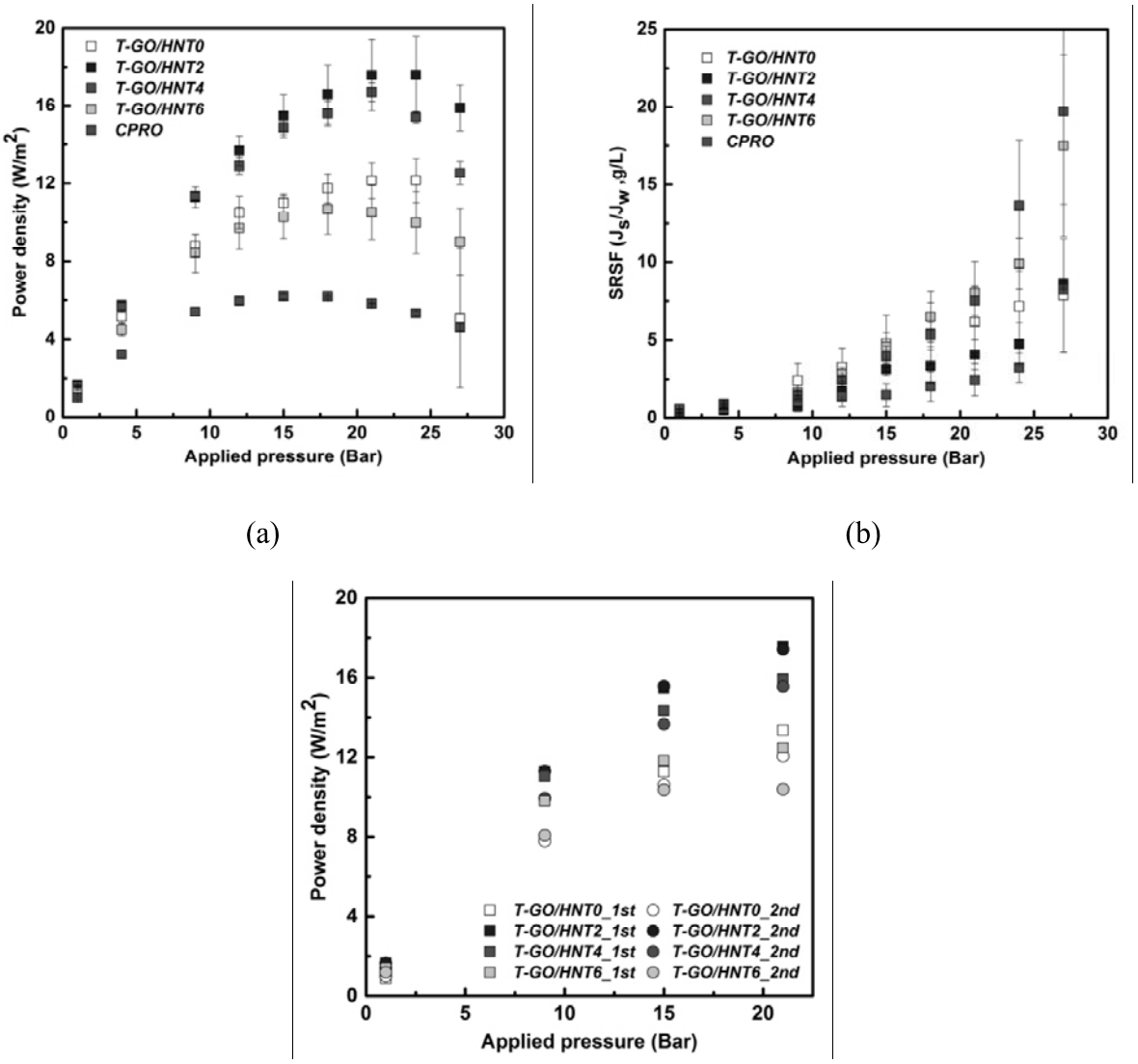

503 **Figure 5** Comparison of PD (a), SRSF (b), and pressure cycling test (c) of *T-GO/HNT0, T-*
504 *GO/HNT2, T-GO/HNT4 and T-GO/HNT6* under different applied hydraulic pressures. The
505 concentration of HNTs in the bottom layer was 0, 2, 4 and 6 wt%, and the GO in the top layer was
506 at 0.25 wt%. The draw and feed solutions were 1 M NaCl solution and DI water, respectively.

507

Long-term performance tests of the membranes were conducted to further investigate the comparative stability of the *T-GO/HNT4* PRO membrane sample with the *T-S/free* sample. Fig. 6 shows the PD and SRSF of *T-S/free* and *T-GO/HNT4* at applied pressures of 18 and 21 bar, respectively, for 300 min. These membranes showed a remarkably stable PD and SRSF during long-term operation, providg further evidence that *T-GO/HNT4* possesses desirable structural properties for stable long-term performance under high pressure, and hence that this membrane offers great potential for practical PRO application.

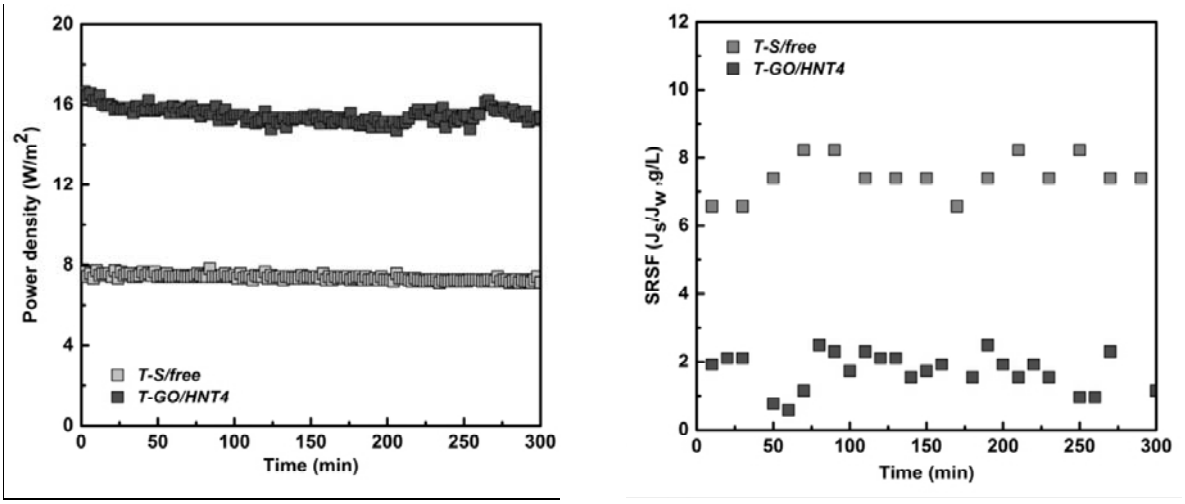

(a) (b)

Figure 6 (a) PD and (b) SRSF of *S/free* and *GO/HNT4* under applied pressures of 18 bar for *T-S/free* and 21 bar for *T-GO/HNT4* for 300 min. The draw and feed solutions were 1 M NaCl solution and DI water, respectively.

3.3 Anti-fouling properties of TFC PRO membranes in PRO processes

3.3.1 Fouling of TFC PRO membranes with alginate and colloidal silica

The fouling tests for each membrane were conducted at the respective hydraulic pressures for optimum PD of the membrane. Fig. 7 depicts the variations of normalized water flux (J_w/J_0) of the synthesized and commercial (*CPRO*) membranes as a function of the accumulated permeate volume (mL) using the alginate-silica mixture as a model foulant under PRO operation. As shown in Fig. 7, the normalized water fluxes of all membranes immediately began to decline rapidly, which can be attributed to membrane fouling and its subsequent impact on the internal concentration polarization in the presence of model foulants [14]. The fouling resistance of the dual-layered PRO membranes improved significantly with the increase of HNT loading in the membrane substrate from 0 to 4 wt%. Although, the initial flux of *T-GO/HNT4* was relatively high in PRO operation, the flux decline rate of the membrane was the lowest during the 3 h fouling test. The normalized flux of *T-GO/HNT4* decreased by only 17% compared to 21% for *T-GO/HNT2,* over 25% for *T-GO/HNT0* and even more drastically to 57% for the *CPRO* membrane, showing the enhanced fouling resistance of the membrane substrates with HNTs incorporated. Consistent with these trends, the bottom surface of *T-GO/HNT4* showed less evidence of foulant (alginate and colloidal silica) deposition on the surface than those of the other membranes, as observed from the SEM images of the bottom surface of fouled PRO membranes presented in Fig. S5.

The excellent fouling resistance properties of *T-GO/HNT4* are likely because of the behavior of the HNTs in the polymer structure. In addition to the formation of a robust membrane substrate structure that prevents the foulant from penetrating into pores of the membrane substrate, the presence of HNTs increases the negative charge on the membrane surface via the presence of

hydroxyl groups (OH^-) on the HNTs, which enhances electrostatic repulsion between the membrane and major foulants such as organic matter, colloidal particles and microorganisms [49, 50]. Moreover, the hydrophilicity results in reduced membrane fouling.

The flux decline of the HNT-free PSf based TFC membrane (*T-GO/HNT0*) was the highest of all the synthesized PRO membranes because of the more open and porous internal morphology compared to single-layered membranes, which facilitates the deposition of foulants of various sizes into the membrane substrate's pores, leading to membrane clogging. Furthermore, the high reverse solute diffusion of *T-GO/HNT0* could accelerate membrane fouling and scaling inside the membrane substrate due to the electrostatic attraction between ions and charged foulants [14]. The normalized flux of *T-GO/HNT6* decreased sharply with a pattern similar to that of *T-GO/HNT0*. It is likely that the structure of *T-GO/HNT6* substrate was compacted and partially damaged during the PRO operation under hydraulic pressure, resulting in the formation of undesirable cracks and voids that create favorable locations for the penetration and accumulation of foulants. The high fouling potential of *T-GO/HNT6* may also be accelerated due to its high SRSF in PRO operation.

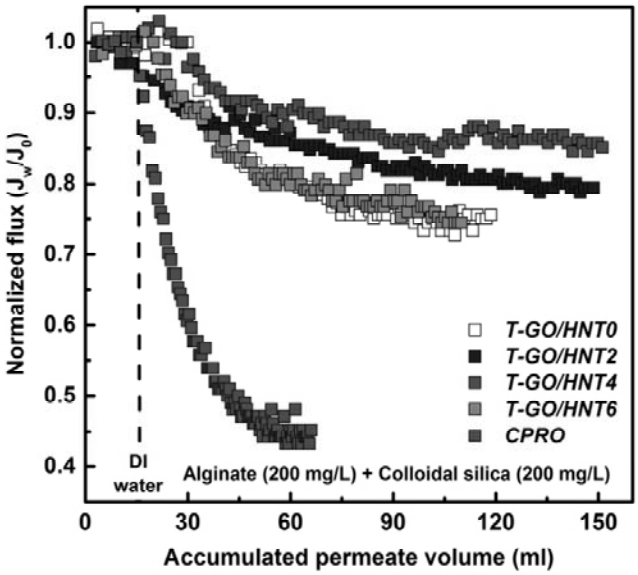

558

559 **Figure 7** Comparison of fouling propensity in the synthesized PRO membranes with different
560 concentrations of HNTs in the bottom layer and the commercial PRO membrane. DI water spiked
561 with sodium alginate (200 mg/L) and colloidal silica (200 mg/L) was used as a feed solution, and
562 the draw solution was a 1 M NaCl solution. The fouling tests for each membrane were conducted
563 at the respective hydraulic pressure at which the PD was largest.

564

565 *3.3.2 Anti-microbial properties of TFC PRO membranes*

566 The anti-microbial activities of the membrane samples to prevent the attachment and
567 growth of bacteria and subsequent biofilm formation (biological fouling) was investigated by
568 incubating viable *E. coli* cells on the surface of membrane samples, using the methods presented
569 in Section 2.6. Fig. 8 presents epifluorescent images of *E. coli* biofilms on a control surface (no
570 membrane substrate) (a), on the top and bottom surfaces of *S/free* as a representative particle-free
571 membrane (b and c) and on top and bottom surfaces of *GO/HNT4* as a representative

572 nanocomposite membrane (d and e). Bacteria were fluorescently stained with the Live/Dead kit,
573 where live bacteria are labeled green and dead bacteria are labeled red. The control in Fig. 8 (a)
574 showed a thin, evenly distributed biofilm of single live cells as well as small micro-sized colonies
575 (clumps of bacteria), and no dead cells could be observed. Similarly, the *S/free* membrane substrate
576 (neat PSf) allowed comparable bacterial attachment and biofilm formation; a single layer of live
577 cells and some small microcolonies could be observed. In contrast, only very few viable *E. coli*
578 cells were observed on the *GO/HNT4* membrane substrate. A few small cell clumps were present
579 on the top surface of the membrane with GO in Fig. 8(d) and some cells, mainly in a single layer,
580 were found on the bottom surface of the membrane with HNTs in Fig. 8(e), suggesting antibacterial
581 activity of the *GO/HNT4* membrane substrate. It is well-known that GO and HNTs in
582 nanocomposite membranes possess bacterial cytotoxicity because of their physico-chemical
583 properties as a hydrophilic, negatively charged and nano-sized intracellular material [42, 51]. This
584 suggests that GO and HNTs in a polymeric membrane can strongly suppress the attachment and
585 biological growth of bacteria on the membrane surface due to their bacterial cytotoxicity, thereby
586 significantly enhancing the membrane's resistance to biological fouling.

587

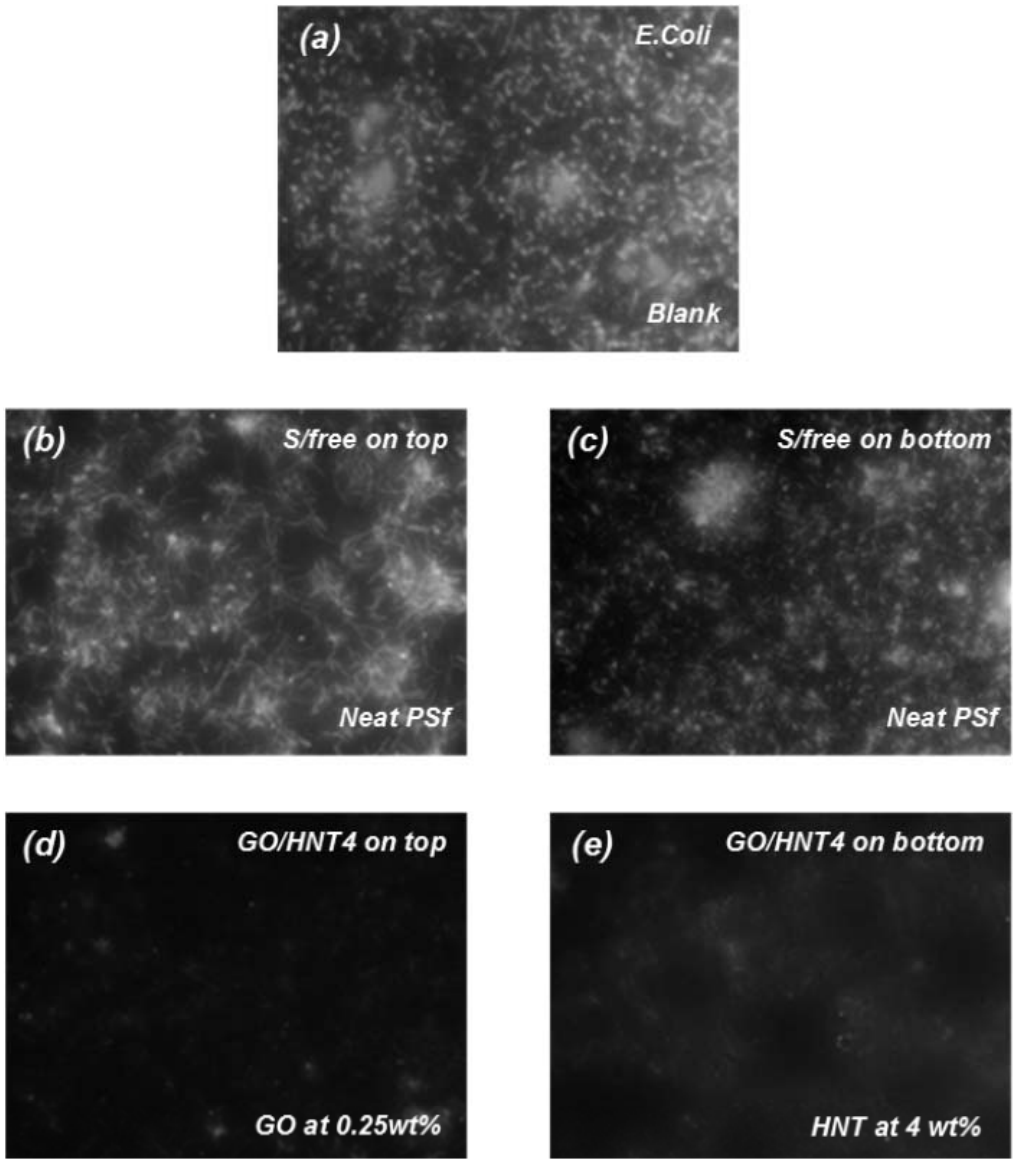

588

589 **Figure 8** Fluorescent images of *E. coli* biofilms, control (a), top and bottom surfaces of *S/free* (b
590 and c), and top and bottom surfaces of *GO/HNT4* (d and e) membrane substrates incubated with
591 *E. coli*.

592

593 **4. Conclusions**

A novel and effective approach has been demonstrated for the preparation of TFC membranes with improved PD, solute selectivity and fouling resistance in PRO processes. The approach involves incorporating GO and HNTs in dual-layered membrane substrates, with a thin PA active layer formed on the GO composite layer. Overall, the newly developed dual-layered GO/HNT nanocomposite membranes exhibited higher PD, low SRSF, and greater mechanical strength than membranes with a pure PSF substrate or a commercial PRO membrane; these are all desirable properties for PRO operation. In addition, the nanocomposite membranes showed outstanding resistance to membrane fouling when subjected to fouling tests with sodium alginate and colloidal silica. The optimum HNT loading for the membrane substrate was 4 wt% and hence the *T-GO/HNT4* membrane showed better performance in terms of osmotic power density and resistance to organic and biological fouling compared to HNT loadings of 0, 2, and 6 wt%, and commercial PRO membranes. The presence of GO and HNTs under optimum loading rates gave the *T-GO/HNT4* membrane a porous inner structure, favorable surface morphology for subsequent PA formation, and excellent mechanical properties allowing it to withstand high hydraulic pressures. In addition, the physico-chemical properties of HNTs in the polymer structure played an important role in enhancing the resistance of the membrane substrate to particulate and biological fouling during PRO operation. The results of this study therefore provide an alternative and effective approach for the fabrication of high-performance PRO membranes for industrial application.

5. Acknowledgements

This research was supported by grants from the Australian Research Council (ARC) Future Fellowship (FT140101208), Qatar National Research Fund under its National Priorities Research Program award number NPRP 10-1231-160069 and the UTS Chancellor's postdoctoral research fellowship. We thank Toray Chemical in Republic of Korea for providing us with the commercial TFC PRO membranes.

6. References

[1] F. Helfer, C. Lemckert, Y.G. Anissimov, Osmotic power with Pressure Retarded Osmosis: Theory, performance and trends – A review, Journal of Membrane Science, 453 (2014) 337-358.

[2] R.E. Pattle, Production of Electric Power by mixing Fresh and Salt Water in the Hydroelectric Pile, Nature, 174 (1954) 660-660.

[3] G. Han, S. Zhang, X. Li, T.-S. Chung, Progress in pressure retarded osmosis (PRO) membranes for osmotic power generation, Progress in Polymer Science, 51 (2015) 1-27.

[4] M. Son, H. Park, L. Liu, H. Choi, J.H. Kim, H. Choi, Thin-film nanocomposite membrane with CNT positioning in support layer for energy harvesting from saline water, Chemical Engineering Journal, 284 (2016) 68-77.

[5] Y. Cui, X.-Y. Liu, T.-S. Chung, Enhanced osmotic energy generation from salinity gradients by modifying thin film composite membranes, Chemical Engineering Journal, 242 (2014) 195-203.

[6] S. Loeb, Production of energy from concentrated brines by pressure-retarded osmosis : I. Preliminary technical and economic correlations, Journal of Membrane Science, 1 (1976) 49-63.

639 [7] A.P. Straub, A. Deshmukh, M. Elimelech, Pressure-retarded osmosis for power generation
640 from salinity gradients: is it viable?, Energy & Environmental Science, 9 (2016) 31-48.
641 [8] G. Han, S. Zhang, X. Li, T.-S. Chung, High performance thin film composite pressure retarded
642 osmosis (PRO) membranes for renewable salinity-gradient energy generation, Journal of
643 Membrane Science, 440 (2013) 108-121.
644 [9] Z.L. Cheng, X. Li, Y.D. Liu, T.-S. Chung, Robust outer-selective thin-film composite
645 polyethersulfone hollow fiber membranes with low reverse salt flux for renewable salinity-
646 gradient energy generation, Journal of Membrane Science, 506 (2016) 119-129.
647 [10] Z.L. Cheng, X. Li, Y. Feng, C.F. Wan, T.-S. Chung, Tuning water content in polymer dopes
648 to boost the performance of outer-selective thin-film composite (TFC) hollow fiber membranes
649 for osmotic power generation, Journal of Membrane Science, 524 (2017) 97-107.
650 [11] N. Lieu Le, M. Quilitzsch, H. Cheng, P.-Y. Hong, M. Ulbricht, S.P. Nunes, T.-S. Chung,
651 Hollow fiber membrane lumen modified by polyzwitterionic grafting, Journal of Membrane
652 Science, 522 (2017) 1-11.
653 [12] Q. She, L. Zhang, R. Wang, W.B. Krantz, A.G. Fane, Pressure-retarded osmosis with
654 wastewater concentrate feed: Fouling process considerations, Journal of Membrane Science, 542
655 (2017) 233-244.
656 [13] Y. Chen, C. Liu, L. Setiawan, Y.-N. Wang, X. Hu, R. Wang, Enhancing pressure retarded
657 osmosis performance with low-pressure nanofiltration pretreatment: Membrane fouling analysis
658 and mitigation, Journal of Membrane Science, 543 (2017) 114-122.
659 [14] G. Han, J. Zhou, C. Wan, T. Yang, T.-S. Chung, Investigations of inorganic and organic
660 fouling behaviors, antifouling and cleaning strategies for pressure retarded osmosis (PRO)

membrane using seawater desalination brine and wastewater, Water Research, 103 (2016) 264-275.

[15] Q. She, Y.K.W. Wong, S. Zhao, C.Y. Tang, Organic fouling in pressure retarded osmosis: Experiments, mechanisms and implications, Journal of Membrane Science, 428 (2013) 181-189.

[16] W.R. Thelin, E. Sivertsen, T. Holt, G. Brekke, Natural organic matter fouling in pressure retarded osmosis, Journal of Membrane Science, 438 (2013) 46-56.

[17] S.C. Chen, C.F. Wan, T.-S. Chung, Enhanced fouling by inorganic and organic foulants on pressure retarded osmosis (PRO) hollow fiber membranes under high pressures, Journal of Membrane Science, 479 (2015) 190-203.

[18] X. Li, S. Zhang, F. Fu, T.-S. Chung, Deformation and reinforcement of thin-film composite (TFC) polyamide-imide (PAI) membranes for osmotic power generation, Journal of Membrane Science, 434 (2013) 204-217.

[19] M. Tian, R. Wang, K. Goh, Y. Liao, A.G. Fane, Synthesis and characterization of high-performance novel thin film nanocomposite PRO membranes with tiered nanofiber support reinforced by functionalized carbon nanotubes, Journal of Membrane Science, 486 (2015) 151-160.

[20] S. Chou, R. Wang, A.G. Fane, Robust and High performance hollow fiber membranes for energy harvesting from salinity gradients by pressure retarded osmosis, Journal of Membrane Science, 448 (2013) 44-54.

[21] Q. She, J. Wei, N. Ma, V. Sim, A.G. Fane, R. Wang, C.Y. Tang, Fabrication and characterization of fabric-reinforced pressure retarded osmosis membranes for osmotic power harvesting, Journal of Membrane Science, 504 (2016) 75-88.

683 [22] Z.L. Cheng, X. Li, Y.D. Liu, T.-S. Chung, Robust outer-selective thin-film composite
684 polyethersulfone hollow fiber membranes with low reverse salt flux for renewable salinity-
685 gradient energy generation, Journal of Membrane Science, 506 (2016) 119-129.
686 [23] N.L. Le, N.M.S. Bettahalli, S.P. Nunes, T.-S. Chung, Outer-selective thin film composite
687 (TFC) hollow fiber membranes for osmotic power generation, Journal of Membrane Science, 505
688 (2016) 157-166.
689 [24] X. Zhang, J. Tian, Z. Ren, W. Shi, Z. Zhang, Y. Xu, S. Gao, F. Cui, High performance thin-
690 film composite (TFC) forward osmosis (FO) membrane fabricated on novel hydrophilic
691 disulfonated poly(arylene ether sulfone) multiblock copolymer/polysulfone substrate, Journal of
692 Membrane Science, 520 (2016) 529-539.
693 [25] A. Qin, X. Li, X. Zhao, D. Liu, C. He, Engineering a Highly Hydrophilic PVDF Membrane
694 via Binding TiO2 Nanoparticles and a PVA Layer onto a Membrane Surface, ACS Applied
695 Materials & Interfaces, 7 (2015) 8427-8436.
696 [26] Y. Zhu, W. Xie, F. Zhang, T. Xing, J. Jin, Superhydrophilic In-Situ-Cross-Linked
697 Zwitterionic Polyelectrolyte/PVDF-Blend Membrane for Highly Efficient Oil/Water Emulsion
698 Separation, ACS Applied Materials & Interfaces, 9 (2017) 9603-9613.
699 [27] X. Li, T. Cai, G.L. Amy, T.-S. Chung, Cleaning strategies and membrane flux recovery on
700 anti-fouling membranes for pressure retarded osmosis, Journal of Membrane Science, 522 (2017)
701 116-123.
702 [28] G. Han, Z.L. Cheng, T.-S. Chung, Thin-film composite (TFC) hollow fiber membrane with
703 double-polyamide active layers for internal concentration polarization and fouling mitigation in
704 osmotic processes, Journal of Membrane Science, 523 (2017) 497-504.

705 [29] H. Salehi, M. Rastgar, A. Shakeri, Anti-fouling and high water permeable forward osmosis
706 membrane fabricated via layer by layer assembly of chitosan/graphene oxide, Applied Surface
707 Science, 413 (2017) 99-108.
708 [30] Y. Li, S. Qi, Y. Wang, L. Setiawan, R. Wang, Modification of thin film composite hollow
709 fiber membranes for osmotic energy generation with low organic fouling tendency, Desalination,
710 424 (2017) 131-139.
711 [31] X. Liu, H.Y. Ng, Double-blade casting technique for optimizing substrate membrane in thin-
712 film composite forward osmosis membrane fabrication, Journal of Membrane Science, 469 (2014)
713 12-126.
714 [32] X. Liu, H.Y. Ng, Fabrication of layered silica–polysulfone mixed matrix substrate membrane
715 for enhancing performance of thin-film composite forward osmosis membrane, Journal of
716 Membrane Science, 481 (2015) 148-163.
717 [33] P. Xiao, L.D. Nghiem, Y. Yin, X.-M. Li, M. Zhang, G. Chen, J. Song, T. He, A sacrificial-
718 layer approach to fabricate polysulfone support for forward osmosis thin-film composite
719 membranes with reduced internal concentration polarisation, Journal of Membrane Science, 481
720 (2015) 106-114.
721 [34] S. Lim, M.J. Park, S. Phuntsho, L.D. Tijing, G.M. Nisola, W.-G. Shim, W.-J. Chung, H.K.
722 Shon, Dual-layered nanocomposite substrate membrane based on polysulfone/graphene oxide for
723 mitigating internal concentration polarization in forward osmosis, Polymer, 110 (2017) 36-48.
724 [35] S. Bano, A. Mahmood, S.-J. Kim, K.-H. Lee, Graphene oxide modified polyamide
725 nanofiltration membrane with improved flux and antifouling properties, J. Mater. Chem. A, 3
726 (2015) 2065-2071.

[36] H.-R. Chae, J. Lee, C.-H. Lee, I.-C. Kim, P.-K. Park, Graphene oxide-embedded thin-film composite reverse osmosis membrane with high flux, anti-biofouling, and chlorine resistance, Journal of Membrane Science, 483 (2015) 128-135.

[37] M.J. Park, S. Phuntsho, T. He, G.M. Nisola, L.D. Tijing, X.-M. Li, G. Chen, W.-J. Chung, H.K. Shon, Graphene oxide incorporated polysulfone substrate for the fabrication of flat-sheet thin-film composite forward osmosis membranes, Journal of Membrane Science, 493 (2015) 496-507.

[38] M. Liu, Z. Jia, D. Jia, C. Zhou, Recent advance in research on halloysite nanotubes-polymer nanocomposite, Progress in Polymer Science, 39 (2014) 1498-1525.

[39] M. Du, B. Guo, D. Jia, Newly emerging applications of halloysite nanotubes: a review, Polymer International, 59 (2010) 574-582.

[40] M.T. Byrne, Y.K. Gun'ko, Recent Advances in Research on Carbon Nanotube–Polymer Composites, Advanced Materials, 22 (2010) 1672-1688.

[41] J.K.W. Sandler, S. Pegel, M. Cadek, F. Gojny, M. van Es, J. Lohmar, W.J. Blau, K. Schulte, A.H. Windle, M.S.P. Shaffer, A comparative study of melt spun polyamide-12 fibres reinforced with carbon nanotubes and nanofibres, Polymer, 45 (2004) 2001-2015.

[42] S. Kang, M.S. Mauter, M. Elimelech, Physicochemical Determinants of Multiwalled Carbon Nanotube Bacterial Cytotoxicity, Environmental Science & Technology, 42 (2008) 7528-7534.

[43] N. Widjojo, T.-S. Chung, M. Weber, C. Maletzko, V. Warzelhan, The role of sulphonated polymer and macrovoid-free structure in the support layer for thin-film composite (TFC) forward osmosis (FO) membranes, Journal of Membrane Science, 383 (2011) 214-223.

748 [44] M. Ghanbari, D. Emadzadeh, W.J. Lau, H. Riazi, D. Almasi, A.F. Ismail, Minimizing
749 structural parameter of thin film composite forward osmosis membranes using
750 polysulfone/halloysite nanotubes as membrane substrates, Desalination, 377 (2016) 152-162.
751 [45] P. van de Witte, P.J. Dijkstra, J.W.A. van den Berg, J. Feijen, Phase separation processes in
752 polymer solutions in relation to membrane formation, Journal of Membrane Science, 117 (1996)
753 1-31.
754 [46] L.D. Tijing, Y.C. Woo, W.-G. Shim, T. He, J.-S. Choi, S.-H. Kim, H.K. Shon,
755 Superhydrophobic nanofiber membrane containing carbon nanotubes for high-performance direct
756 contact membrane distillation, Journal of Membrane Science, 502 (2016) 158-170.
757 [47] M. Ionita, A.M. Pandele, L. Crica, L. Pilan, Improving the thermal and mechanical properties
758 of polysulfone by incorporation of graphene oxide, Composites Part B: Engineering, 59 (2014)
759 133-139.
760 [48] I. Zaman, T.T. Phan, H.-C. Kuan, Q. Meng, L.T. Bao La, L. Luong, O. Youssf, J. Ma,
761 Epoxy/graphene platelets nanocomposites with two levels of interface strength, Polymer, 52 (2011)
762 1603-1611.
763 [49] X. Li, T. Cai, T.-S. Chung, Anti-Fouling Behavior of Hyperbranched Polyglycerol-Grafted
764 Poly(ether sulfone) Hollow Fiber Membranes for Osmotic Power Generation, Environmental
765 Science & Technology, 48 (2014) 9898-9907.
766 [50] M. Hu, S. Zheng, B. Mi, Organic Fouling of Graphene Oxide Membranes and Its Implications
767 for Membrane Fouling Control in Engineered Osmosis, Environmental Science & Technology, 50
768 (2016) 685-693.

[51] Q. Zhao, J. Hou, J. Shen, J. Liu, Y. Zhang, Long-lasting antibacterial behavior of a novel mixed matrix water purification membrane, Journal of Materials Chemistry A, 3 (2015) 18696-18705.

Supporting information

Dual-layered nanocomposite membrane incorporating graphene oxide and halloysite nanotube for high osmotic power density and fouling resistance

Sungil Lim[1], Myoung Jun Park[1], Sherub Phuntsho[1], Anne Mai-Prochnow[2], Anthony B. Murphy[2], Dong Han Seo[2] and Hokyong Shon[1] *

[1]*Centre for Technology in Water and Wastewater (CTWW), School of Civil and Environmental Engineering, University of Technology Sydney (UTS), Australia*

[2] *Commonwealth Scientific and Industrial Research Organisation (CSIRO) Manufacturing, Australia*

* Corresponding author: A/Prof. Hokyong Shon Email: hokyong.shon-1@uts.edu.au; Tel.: +61 2 9514 2629; Fax: +61 2 9514 2633.

1. Formation of thin-film composite membranes

The surface of the membrane substrates was properly cleaned using an air knife supplied with nitrogen gas to remove any solid impurities and liquid molecules that may be present. In the IP process, the substrate was firstly soaked in the MPD solution at 4.0 wt% for 150 s, and the excessive MPD solution on the substrate surface was then completely removed with the help of air knife. A TMC solution at 0.1 wt% mixed with high purity n-hexane was then contacted on the surface of the MPD-soaked membrane substrate for 60 s to form the PA active layer. The excessed TMC solution was subsequently drained off and the membrane was then air-cured for 20 min by simply exposing to the room temperature. After the curing process, the nascent membranes were rinsed with DI water to remove any unreacted monomer from the substrate and then stored in DI water before performance tests. The resultant membranes denoted as TFC membranes were characterized and evaluated for PRO performance.

2. Evaluation of intrinsic transport properties of thin-film composite membranes

The pure water permeability (A, $Lm^{-2}h^{-1}bar^{-1}$) and solute permeability coefficient (B, $Lm^{-2}h^{-1}$) of the TFC PRO membranes were measured using a cross-flow RO test unit with the effective membrane area at 20.02 cm^2. Prior to the experiment, all samples were firstly operated in a cross-flow mode at 5 bar using deionized water in order to minimize the effect of membrane compaction. All tests were subsequently conducted at a trans-membrane pressure of 5 bar, cross-flow velocity of 16.7 cm/s and at constant temperature of 23±0.5°C. The A value of the TFC membranes was determined using DI water as feed at 5 bar while the salt rejection of (R) was determined using 1,000 ppm NaCl as the feed. The values of A, R and B were

calculated using Eq. 1, 2 and 3, respectively. Where ΔP is the trans-membrane pressure, J_w is the permeate water flux whereas C_p and C_f are the NaCl concentrations of permeate and feed streams in the test, respectively.

$$A = \frac{J_w}{\Delta P} \tag{1}$$

$$R = \left(1 - \frac{C_p}{C_f}\right) \times 100\% \tag{2}$$

$$B = J_w \frac{1-R}{R} \exp\left(-\frac{J_w}{k}\right) \tag{3}$$

The value of B was calculated using the mass transfer coefficient k of the membrane under the RO test which obtained based on Eq. 4.

$$k = \frac{Sh \cdot D}{d_h} \tag{4}$$

where D and d_h are the solute diffusion coefficient and the hydraulic diameter of the cross-flow membrane cell, respectively. The Sherwood number (Sh) was determined with Eqs. 5 and 6 using Reynolds number (Re) and Schmidt number (Sc) in a rectangular channel with characteristic length L [1].

$$Sh = 1.85\left(Re \cdot Sc \frac{d_h}{L}\right)^{0.33} \quad \text{(Laminar flow as } Re < 2000\text{)} \tag{5}$$

$$Sh = 0.04\left(Re^{0.75} \cdot Sc^{0.33}\right) \quad \text{(Turbulent flow as } Re > 2000\text{)} \tag{6}$$

3 Evaluation of TFC PRO membrane performances (Water flux, reverse solute flux and power density)

The performances of PRO membranes were tested by using a laboratory-scale PRO test unit. The PRO test unit consists of stainless-steel based membrane test cell containing two water channels on each side of the membrane with an effective area of 20.02 cm^2 and channel thickness of 3 mm. The FS and DS were supplied on each channel in a co-current mode by using a gear pump (Cole Parmer, USA) and high-pressure pump (BM-4.18, BTLN, China), respectively. The temperature of the FS and DS was fixed at 23 °C constantly by using the temperature control system. The cross-flow velocity in the performance tests was set at 6.4 cm/s (0.3 L/min). The orientation of the membrane in the test was AL-DS (active layer facing draw solution). All PRO membranes were stabilized at 10 bar for 1 h prior to the PRO tests. The applied hydraulic pressure in the draw stream was varied from 0 to 27 bar in the PRO tests. In the PD tests, DI water was used as FS while 1 M NaCl was used as DS. As shown in Eq. 7 and 8, the water flux (J_w) and reverse solute flux (J_s) were determined by measuring the change in the volume and concentration of the FS reservoir, respectively. The changed volume of FS as a function of the time interval (Δt) is presented as ΔV_{draw}. A_m is the effective membrane surface area.

$$J_w = \frac{\Delta V_{draw}}{A_m \Delta t} \tag{7}$$

The J_s of the membrane was defined using Eq. 8 as follows:

$$J_s = \frac{\Delta C_{t,feed} V_{t,feed}}{A_m \Delta t} \tag{8}$$

where $\Delta C_{t,feed}$ and $V_{t,feed}$ are the change in salt concentration of the FS and the volume of FS reservoir at 2 L after the duration of time (Δt), respectively.

As shown in Eq. 9, the specific reverse solute flux (*SRSF*, J_s/J_w) is defined as the ratio of water flux and reverse solute flux for the PRO membranes.

$$SRSF = \frac{J_s}{J_w} \tag{9}$$

With the values of the water flux as a function of the trans-membrane pressure, the PD (*W*, W/m^2) as an important value to estimate the energy production in PRO processes was determined by the product of water flux (L) across the membranes and the trans-membrane pressure (bar). The PD is derived in Eq. 10 as below: [2]

$$W = \frac{J_w \times \Delta P}{36} \tag{10}$$

4. List of figures

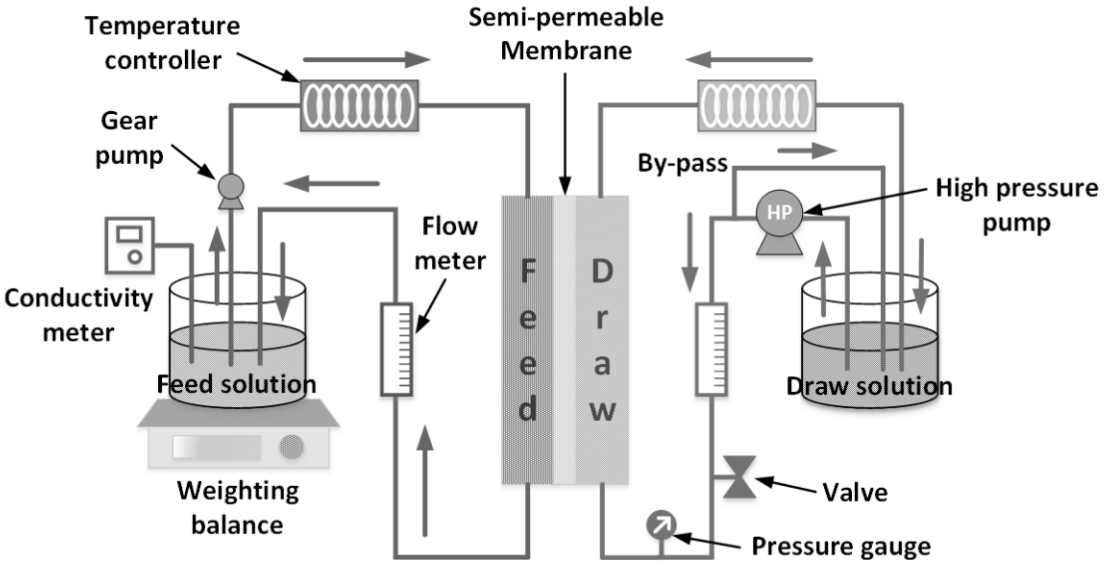

Figure S1 Schematic illustration of the laboratory-scale PRO membrane test unit.

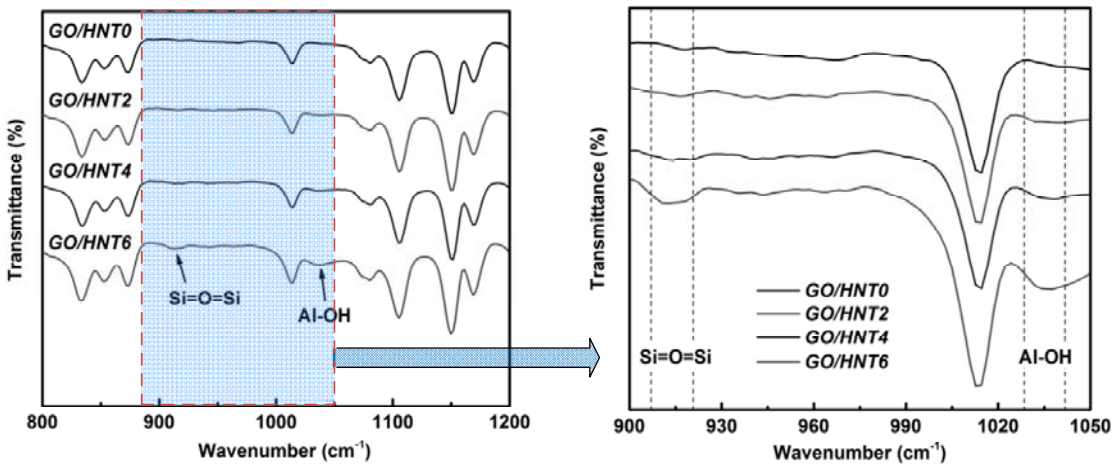

Figure S2 ATR-FTIR spectra for dual-layered GO/HNT hybrid PRO membranes in the range of 800 and 1200 cm^{-1}.

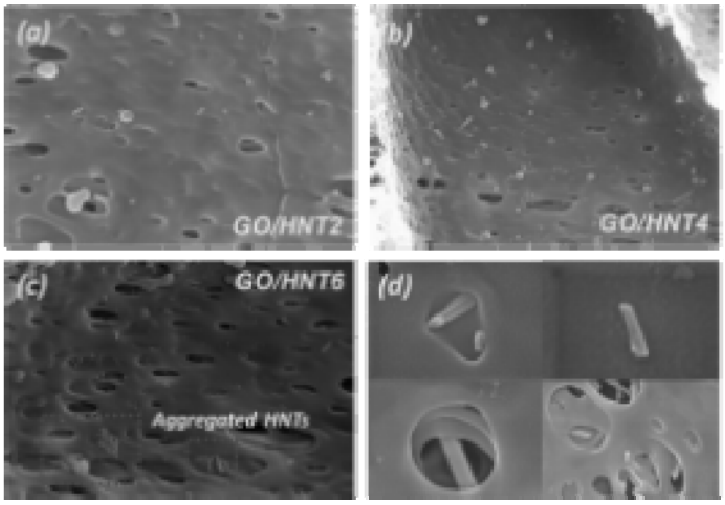

Figure S3 Existence of HNTs on the bottom layer of flat-sheet PRO membranes: (a) *GO/HNT2*, (b) *GO/HNT4*, (c) *GO/HNT6*, and (d) High magnitude images of HNTs in the pores of PRO membranes.

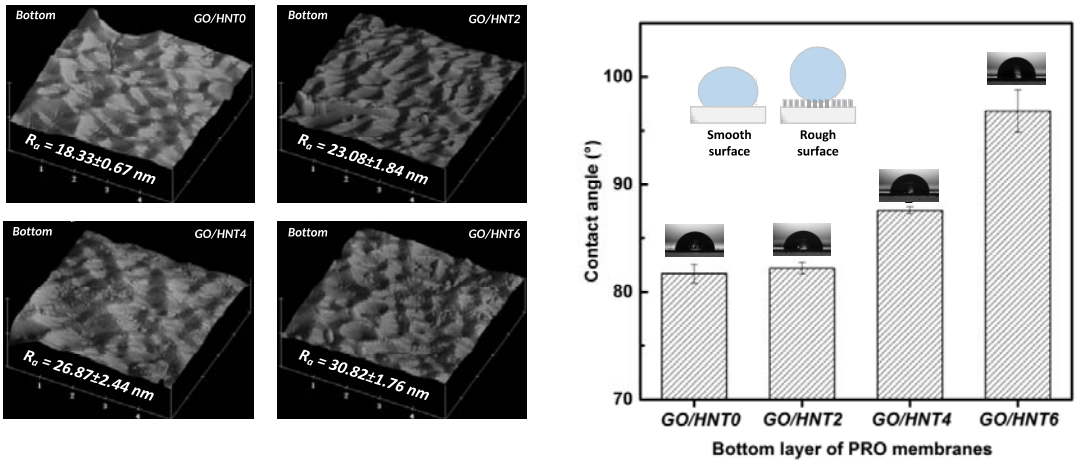

(a) (b)

Figure S4 (a) 3D AFM images / average roughness, and (b) contact angle of the bottom surface of flat-sheet PRO membranes prepared different HNT loadings: *GO/HNT0, GO/HNT2*, *GO/HNT4* and *GO/HNT6*. The values of contact angle in random positions were averaged with the data of five measurements in random positions each samples.

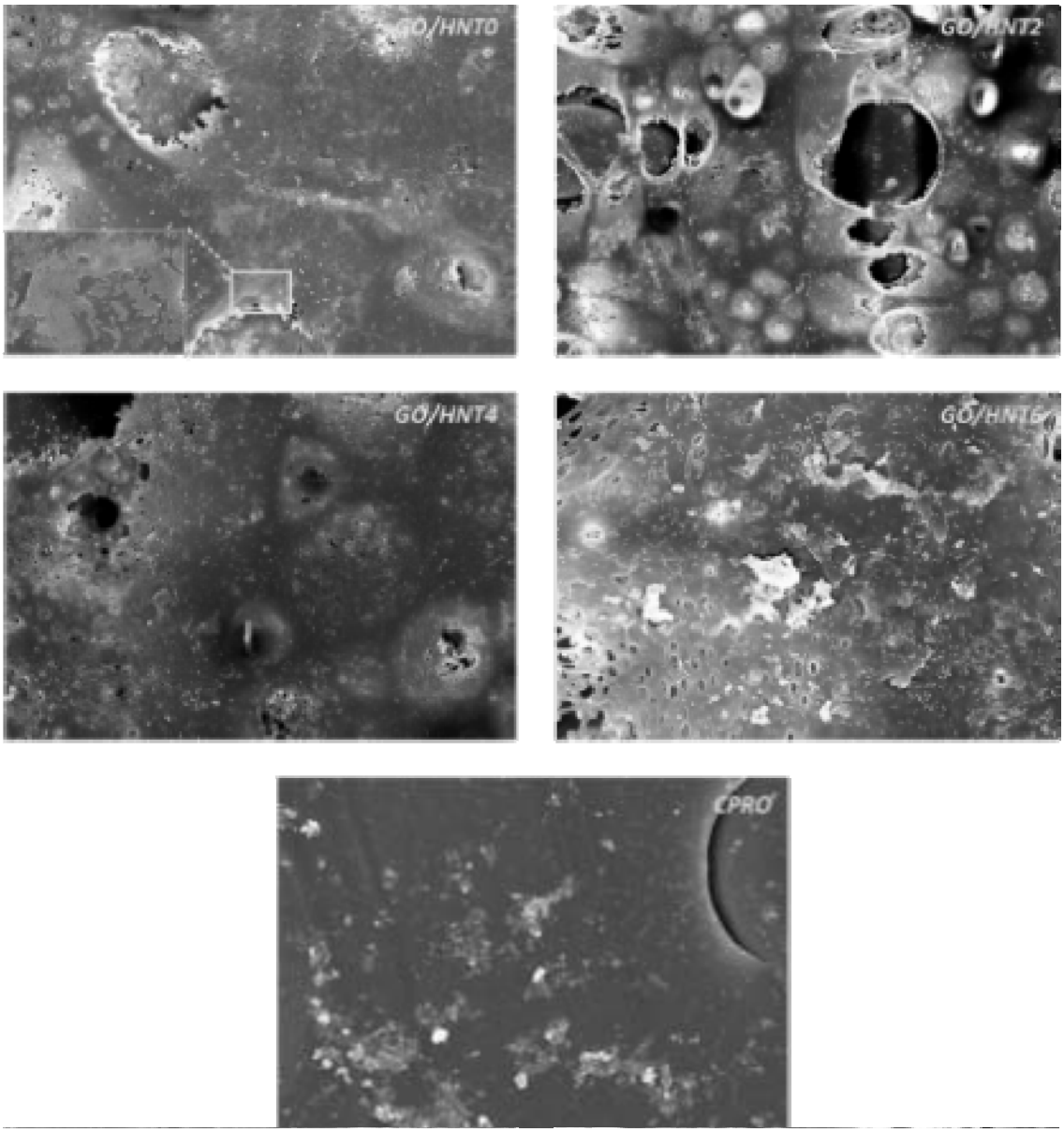

Figure S5 SEM images of the bottom surface of fouled PRO membranes: *GO/HNT0*, *GO/HNT2, GO/HNT4, GO/HNT6* and *CPRO*.

5. References

[1] C.H. Tan, H.Y. Ng, Revised external and internal concentration polarization models to improve flux prediction in forward osmosis process, Desalination, 309 (2013) 125-140.

[2] G. Han, J. Zhou, C. Wan, T. Yang, T.-S. Chung, Investigations of inorganic and organic fouling behaviors, antifouling and cleaning strategies for pressure retarded osmosis (PRO) membrane using seawater desalination brine and wastewater, Water Research, 103 (2016) 264-275.